INSTITUTE OF PHYSICS PUBLISHING PHYSICAL BIOLOGY
Phys. Biol. **3** (2006) 93–100 doi:10.1088/1478-3975/3/2/001

A cellular automaton model for the migration of glioma cells

M Aubert[1], M Badoual[1], S Féreol[2], C Christov[3] and B Grammaticos[1]

[1] GMPIB, Université Paris VII, case 7021, 75251 Paris, France
[2] Unité INSERM 492 (IM3), 94010 Créteil, France
[3] Plateforme d'Imagerie Cellulaire et Tissulaire de l'IFR10, Institut Mondor de Médecine Moléculaire, Paris, France

Received 9 December 2005
Accepted for publication 27 March 2006
Published 13 April 2006
Online at stacks.iop.org/PhysBio/3/93

Abstract
We present a study of *in vitro* cell migration in two dimensions as a first step towards understanding the mechanisms governing the motility of glioma cells. Our study is based on a cellular automaton model which aims at reproducing the kinetics of a lump of glioma cells deposited on a substrate of collagen. The dynamical effects of cell attraction and motion inertia are introduced through adequate automaton rules. We compare the density profiles given by the model to those obtained experimentally. The result of the best fit indicates a substantial cell–cell attraction due to cell–cell communication through gap junctions (or chemotaxis) and negligible inertia effects during migration. Tracking of individual migrating cells indicates highly convoluted cell trajectories.

1. Introduction

In contrast to normal tissues, malignant tumours are characterized by unrestrained proliferation and invasion that perturb first local and ultimately general tissue homoeostasis. Although clinically and biologically diverse, all malignant tumours grow by cell proliferation creating an abnormal bulk and invading host tissues thereby assuring tumour cell spread. Numerous modelling studies have set out to define the general rules underpinning the growth behaviour of tumours (see [1, 2] for reviews of modelling approaches and tissue-specific examples). In the case of gliomas, invasion (cell diffusion) is a major component of tumour growth, together with cell proliferation. This is the main conclusion of the prototypical modelling study of Burgess *et al* [3]. These authors have introduced a simple model for glioma growth based on cell proliferation and cell diffusion from an initial tumour lump. Their assumptions are spherical symmetry, homogeneous diffusion and exponential growth, incorporated in the equation:

$$\frac{\partial \rho}{\partial t} = D\nabla^2\rho + \kappa\rho. \tag{1.1}$$

The Burgess model stipulates that glioma growth results from an interplay between cell diffusion and cell proliferation. It is through cell migration (diffusion) that gliomas occupy progressively vaster regions in the tumour-harbouring brain; cell proliferation is responsible for the formation of tumour bulk. This very general concept of tumour kinetics is in accord with most clinical and experimental data (for reviews see [8, 9]). Moreover, this model appears valid whatever the presumptive driving forces of glioma invasion: intrinsic abnormal high motility of glioma cells [4], influence of chemotactic and growth factors [5], availability of nutrients [1], or anaerobic metabolism gradients [6, 7]. These numerical studies are largely corroborated by numerous clinical and experimental observations (for reviews see [8, 9]) pointing to the unique locally invasive behaviour of gliomas. From the very onset of their development, these tumours, commonly consisting of a central bulk and halo of diffusely invasive cells, fan out to distant areas of the brain (e.g. the contralateral brain hemisphere), largely defeating the effect of surgery and other local therapies [8]. Left-out infiltrated cells were shown to be the substrate of the inevitable and ultimately fatal glioma recurrences after surgery.

The model of Burgess *et al* and subsequent work based on its reasoning (e.g. [10]) examine invading glioma cells at the level of the tumour itself where diffusion is the main component of tumour growth. However, important insights

into the invasive properties of gliomas could also be gained by examination of the behaviour of migrating single cells or population of cells *in vitro*, and indeed several methodological approaches have been applied [4, 5, 9, 11, 12]. In order to understand diffusion as a kinetic parameter, it is but natural to consider its source, namely the motility of the glioma cells.

The present work is devoted to the study of the diffusion properties of glioma cells during migration. As such, our study does not aim at a description of *in vivo* glioma growth neither do we pretend that our results can be directly extrapolated to a realistic situation. Here we are concentrating on questions of two-dimensional diffusion of glioma cells over a collagen substrate, examining the motility of cells and their interaction. Our cell spheroids contain cells counted in hundreds, rather than the billions in a real glioma, the period of study is limited to 48 h rather than months or years; and moreover, no significant proliferation or apoptosis is present. The diffusion properties of glioma cells will be examined in the theoretical part of our study with the help of a cellular automaton. Models based on cellular automata have already been considered for the description of tumour growth [2, 13, 14]. Here, however, we shall be limiting ourselves to the study and modelling of the migration alone (no net proliferation and no necrosis). The advantage of an approach based on a cellular automaton is that the latter is a dynamical system with simple dynamics.

Malignant tumour cells *in vivo* can have interaction with other tumour cells and also with normal astrocytes. This interaction could play a role in tumour growth and tumour invasiveness. One example of cell interaction that exists in the case of gliomas is gap junction mediated attraction. For instance, gap junctions exist between tumour cells as well as between tumour cells and normal astrocytes [15]. It is still not clear which interaction is involved in tumour growth (perhaps both). In a recent study, it has been shown that the tumour cell–tumour cell gap junctional communication (GJC) and the tumour cells–astrocyte GJC could play different roles [16]. In this paper, we decided, for simplicity, to restrict our study to interactions between tumour cells. Thus, we studied the migration of tumour cells on a collagen substrate, where only tumour cell interactions are possible.

The various effects can be incorporated with the help of some simple well-chosen rules. The numerical simulations are not particularly demanding and the interpretation of results is straightforward in most cases. The results of the model will be compared to experimental data obtained with the method summarized below. We show that data analysis by means of a cellular automaton model makes possible the formulation of hypotheses concerning the motility of glioma cell as well as their interaction.

2. Materials and methods

2.1. Cell lines and spheroids

In these experiments, we used a highly motile established human glioma cell line (GL15) extensively studied in [16–18]. Spheroids were derived through the overlay-culture methods as previously described [18]. Briefly, GL15 cells from trypsinized stock flasks were seeded at 2×10^4 cell cm^{-2} in 3 ml of GL15 culture in 3.5 cm Petri dishes coated with an attachment limiting surface (agar). Cells were kept in a standard cell culture incubator and approximately half of the overlay medium was discarded and replenished with a fresh medium every other day. Under these conditions, GL15 cells form spheroids (200–1200 μm in diameter) in 10–14 days.

2.2. Migration-out-of-spheroid assay

For the migration assay, the bottoms of standard 3.5 cm Petri dishes were coated with collagen IV, a substrate permissive for glioma cell migration during 12 h at room temperature. Collagen IV aliquots were thawed at 4 °C overnight, diluted in sterile water, and poured into the Petri dishes; the concentration chosen corresponded to 1 μg cm^{-2}, assuming that all of the collagen IV present in the solution was absorbed on the polystyrene surface. After the collagen IV solution was aspirated, bottoms of the dishes were covered with a thin layer of sterile BSA. Individual spheroids selected under an inverted microscope were pipetted onto the bottom of the Petri dish in 200 μl of a GL15 medium, and left in a incubator for 6 h to allow spheroid attachment, after which 3 ml of a fresh GL15 medium was added. Microscopic observation began at $t_0 = 6$ h when cell viability and spheroid attachment were verified and lasted 48 h during which time spheroids were photographed at 12 h intervals (t_0–t_4) using an inverted Leica microscope coupled with a Coolsnap CCD camera. Cells were kept in a standard cell incubator between observations. During these experiments, the rate of cell proliferation (assessed by the proportion of cells in S-phase as demonstrated by BrDU incorporation) is around 5% and is nearly compensated by the rate of apoptosis around 3%, (assessed by nuclear morphology after DAPI nuclear staining). We designed another set of experiments to evaluate cell velocity and paths of individual migrating cells in time-lapse mode. Cells incubated in an environmental chamber mounted on an inverted Axiophot 2 miscroscope were photographed as phase-contrast images every 10 or 20 min for up to 5 h with an AxioCam CCD using the time-lapse option of AxioVision 3.0 (all software and hardware was from Zeiss, Germany). The field of observation corresponded to a microscopic field ($\times$20) selected in immediate vicinity to the spheroid. All cells entirely present in field during the observation period were tracked.

2.3. Treatment of experimental results

Four typical photographs of spheroids and migrating cells are shown in figure 1. In order to extract the density profiles of the cell distribution, we superimposed on each photo, at various times, a system of concentric circles, closely spaced. We then counted the number of cells in each circular ring. Since we have worked throughout with spheroids that were not completely depleted after the 48 h evolution, a central zone of each picture was excluded since it corresponded to the diffusing spheroid. In figure 2, we show the density profiles obtained from the various photographs at times 12, 24, 36 and 48 h after t_0. In figure 3, we also present, superimposed, the

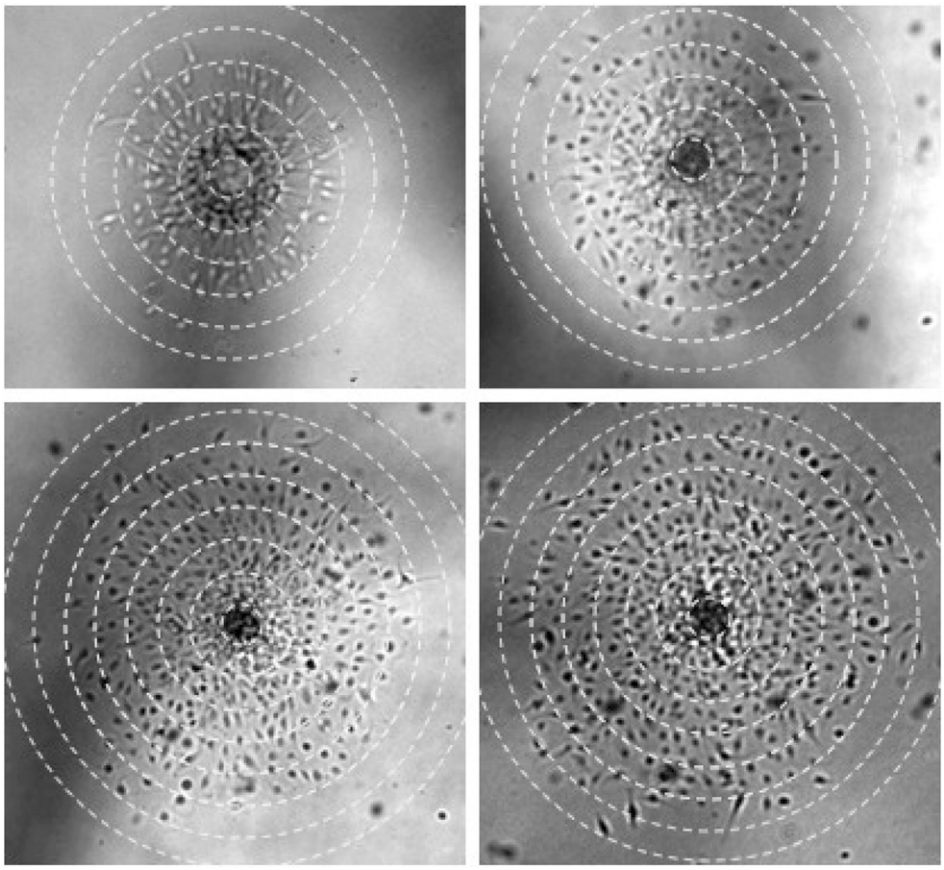

Figure 1. Cell migration pattern over 12, 24, 36 and 48 h, starting from an initial spheroid.

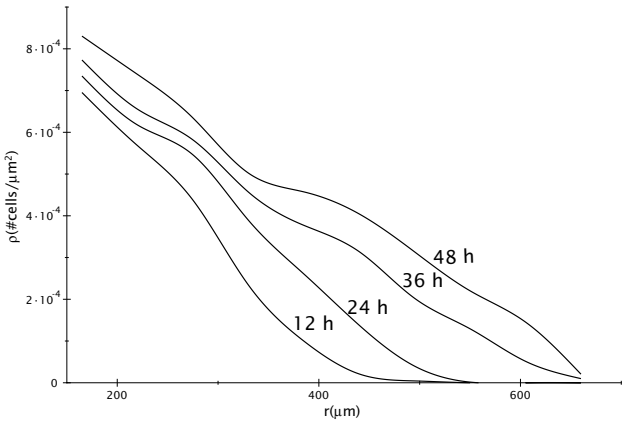

Figure 2. Experimental density profiles obtained after 12, 24 36 and 48 h.

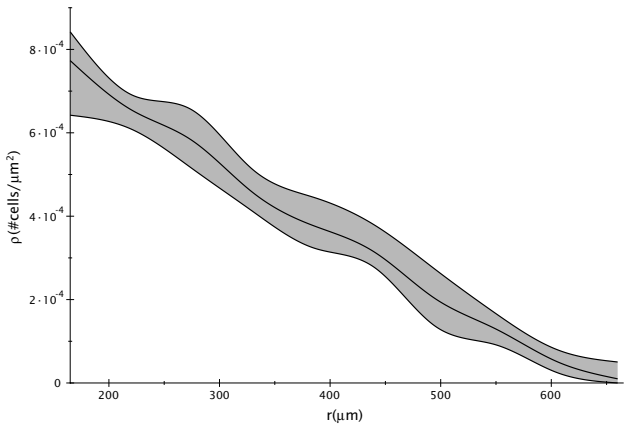

Figure 3. Mean density at 36 h together with the upper and lower density profiles.

upper and lower density profiles obtained at the same moment of the evolution in order to give an idea of the dispersion of the data.

To determine velocities and migration paths in the time-lapse experiments, phase-contrast images of cells were segmented using edge-detection algorithms (KS400 3.0 image analysis software). Typically, for each cell, at each time-point, several (up to 5) binary mask images were obtained by detecting edges of different shallowness and space gradient (valley algorithm). These images of cell contour fragments were then combined by means of an XOR logical operator. The summed final image, manually corrected if necessary, represented the entire cell contour, permitting us to define the centre of gravity (mass) of the cells. Displacements of this centre were used to calculate short-term (20 min) and long-term (5 h) mean velocities, as well as the paths of individual migrating cells. The distributions obtained have been fitted by a Gaussian $a\,\mathrm{e}^{(v-v_0)^2/\sigma^2}$ yielding estimates for the median values of the two mean velocities (as well as of the width of the distributions). The quantity we are particularly interested in is

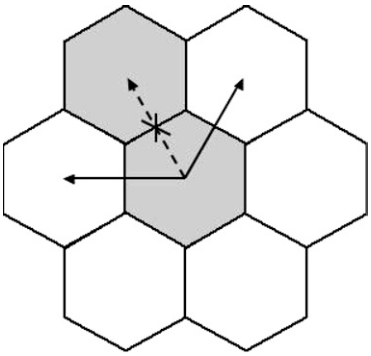

Figure 4. Example of a possible cell move. A grey hexagon denotes the presence of a glioma cell. The cell does not move to an occupied hexagon. In the case of maximal attraction the cell can only move next to an occupied hexagon i.e. in a hexagon shown by a continuous arrow.

the ratio of the medians for the long- and short-interval mean velocities. This ratio is a measure of the complexity of the trajectory of the centre of mass of the cell. The value obtained for the experimental data we analysed was 5.2, indicating a really 'crooked' trajectory.

3. The model

3.1. The geometry

The cellular automaton we shall introduce here for the description of the glioma cell migration is based upon a hexagonal lattice. This choice was dictated by the fact that the hexagonal lattice is the most isotropic among all lattices that pave the plane periodically. The centres of the hexagons form a triangular lattice. Thus, in order to define the position of the centre of a given hexagon, we can introduce three coordinates along axes in $2\pi/3$ angles with respect to each other. If we normalize the coordinates by the distance a between the centres of two adjacent hexagons, the three coordinates become integer numbers i, j and k. Such a system is *a priori* redundant but it suffices to remark that a point with $i = j = k$ is equivalent to $(0, 0, 0)$. Thus any triplet (i, j, k) is equivalent to $(i-k, j-k, 0)$ and we are reduced to just two coordinates.

3.2. The evolution

Each hexagon can be occupied by a single cell at any given time. Thus a cell may move only to a free hexagon. At each update of the automaton we define a random order of all ejected cells and then we evolve them one after the other. When the position of a cell is to be updated a new position among its six neighbours is chosen. If this position is occupied, the cell does not move (shown in figure 4 by the crossed-out dashed arrow). A central part of the lattice is occupied by the equivalent of the glioma cell spheroid, which, we assume, may eject an unlimited number of cells. Once a free position in the hexagons surrounding the centre is created, it is immediately occupied by a cell 'ejected from the centre'. Cell proliferation is not considered since we have seen *in our experimental conditions* that the processes of mitosis and apoptosis practically cancel out.

The rules we have just described would correspond to diffusion of cells without interaction other than that imposed by the constraint of a single cell per hexagon. However, this motion is not quite realistic when it comes to describing living cells. Thus we further introduced more dynamical rules in our 'box and ball' system [19].

The first effect that we included in the model is that of cell attraction. The attraction factor between tumoural cells could include several effects. This factor could account for cell–cell attraction through the cadherin–catenin system, homotype chemotaxis or cell–cell communication through gap junctions. Cadherin are membrane proteins which mediate homotype cell adhesion. It has been suggested that instability and disorganisation of cadherin-mediated junctions favours migration and invasiveness in glioblastoma cell lines [20]. Sander and Deisboeck [5] suggested that the production of an autocrine/paracrine stimulus promotes attraction between cells (homotype chemoattraction). Finally, gap junctions could also account for the attraction factor between cells. In almost all mammalian tissues, cells in contact can directly exchange ions and small molecules through intercellular channels known as gap junctions. GJC is believed to be involved in the regulation of cell proliferation, differentiation and apoptosis. Many tumour-promoting agents such as oncogenes or growth factors inhibit GJC. The expression of gap junction proteins (connexins), particularly cx43, is frequently decreased in brain cancer cells [21] and restoration of GJC by transfection of cx43 genes reverses the transformed phenotype in many types of cancer cells, including rat C6 glioma [22]. Apart from their role in gap junction formation, it has been shown that connexins also have adhesive properties and have been associated with the property of glioma cells to aggregate [23].

The way we are accounting for cell attraction in our model is to favour motion towards a hexagon next to one occupied by a cell. We introduce a threshold p (a number between 0 and 1) and for each evolution pick a random number r between 0 and 1. If $r < p$ the cell moves to a position with occupied nearest neighbours and the opposite if $r > p$. At this point we considered two strategies. The first is that if the chosen motion is impossible, the cell does not move. With these assumptions a threshold $p > 0.5$ corresponds to cell attraction ($p = 1$ i.e. maximum cell attraction, means that a cell can only move to a position next to an occupied one, as shown in figure 4 by the continuous arrows), while $p < 0.5$ corresponds in fact to cell repulsion. The second strategy forces the cell to move, provided there is an adjacent free hexagon. As we shall see in the analysis of the model, experimental results seem to favour the former strategy.

The second effect considered in the model is that of inertia, by which we mean that when cells migrate they may tend to keep the same direction of motion over a distance of some cell diameters. The consequence of this inertia is that a cell cannot abruptly reverse its direction of motion. We have implemented this feature in the model by allowing movement only in the forward direction i.e. keeping the memory of the

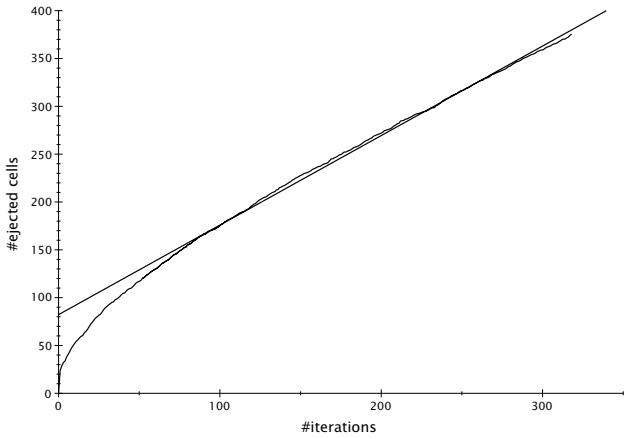

Figure 5. Number of ejected cells as a function of the automaton iterations together with the best linear fit (obtained by neglecting the first 100 iterations).

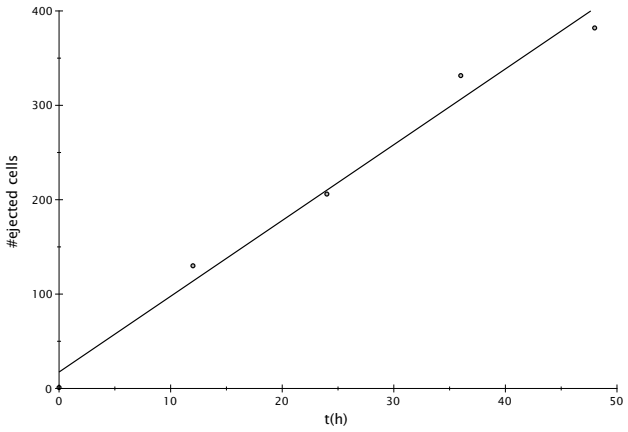

Figure 6. Number of ejected cells as a function of time, obtained from the experiment.

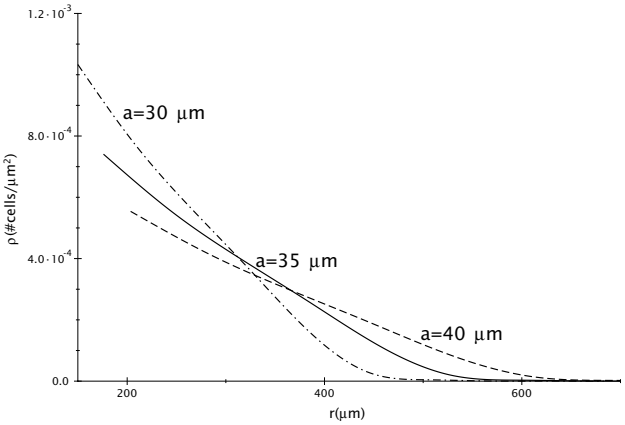

Figure 7. Density profiles for the automaton results, for various values of the lattice spacing.

latest movement of the cell and allowing it to move only towards the three hexagons that are in the forward direction.

The notion of inertia in the motion of a cell is first a physical concept based on the idea that an extended object cannot suddenly reverse the direction of its motion. But inertia could also be due to cellular signalling, as suggested by Deisboeck *et al* [24]. They recently showed that if cells from different types of gliomas have very dispersed velocities [25, 26], these velocities are positively correlated with higher directionality in the cell migration paths [24]: a higher average velocity calculated on a short time scale (10 min) corresponds to a more linear trajectory (plotted on a long time scale of 24 h). For simplicity, we decided to choose one spatial step of the automaton as the 'memory' distance. We believe that a more pronounced motion inertia would not improve our density comparisons.

4. Calibration of the model

In order to be able to compare the results of the experiment to that of the automaton it is necessary to establish a correspondence between the two physical quantities which play a role in both, namely time and space.

4.1. Time calibration

It is clear that the number of updates of the automaton does not have any immediate physical meaning. The quantity that we can easily link to physical time is the number of ejected cells. In figure 5, we give the dependence of the latter on the automaton updates. We can infer from this graphic that the relation is essentially linear (except at the very beginning of the evolution, for which we do not have experimental data). Next we turn to the experimental results and examine the dependence of the number of ejected cells on physical time. From figure 6, we conclude that the relation is, again, roughly linear. Thus the number of the automaton updates can be related to physical time in a straightforward way through the relation of both to the number of ejected cells.

4.2. Space calibration

Concerning space calibration the main difficulty stems from the fact that we assume in our model that the cells occupy hexagons of the same size while in practice both cell size and shape vary. Thus we are led to define an effective cell diameter which can be related to the lattice parameter. We start by remarking that the experimental mean cell density ρ, typically in a circular ring, is given as the number of cells per unit surface. The quantity that comes naturally from the automaton, on the other hand, is d, the number of the occupied sites divided by the number of sites available. In order to relate the latter to the former, it suffices to divide by the surface of an elementary hexagon which, in terms of the lattice parameter (distance between two centres) a, is given by $s = \sqrt{3}a^2/2$. We expect the parameter a to be roughly equal to the effective cell diameter.

In order to assign a value to a we compare the experimentally obtained density profile $\rho(r)$ to that given by the automaton $d(r)/s$ for various values of a. We point out here that, in the case of the automaton, the distance from the centre of the spheroid is measured in lattice spacings n. In order to convert it to a length we must multiply it by the lattice size a, i.e. $r = na$. In figure 7, we compare the density profiles given

by the automaton for various values of a. Since the profile is rather sensitive to the value of a we can by inspection infer a value for the latter, resulting in $a \approx 35\ \mu$m.

5. Results

Having fixed the model and its parameters, we can now present some typical simulation results. The size of the initial spheroid is chosen in accordance with that observed experimentally: a mean diameter of 220 μm, which corresponds roughly to six–seven cells across.

In figure 8 we present cell migration snapshots, starting from the same initial spheroid, at the end of 48 h obtained for different values of the threshold p (as explained in section 3) while neglecting the inertia effect. We give three representative situations for probabilities 1, 0.5 and 0, respectively. The case $p = 1$ corresponds to maximal cell attraction, $p = 0.5$ is close to pure diffusion while $p = 0$ is a situation where cells are repelled rather than attracted (a biologically unrealistic behaviour). As expected, lowering p leads to more diffuse distributions, corresponding to increased motility.

The corresponding density profiles are shown in figure 9. It is clear that the sensitivity with respect to the value of p is so large that one expects to be able to extract a value for p from the best fit of the experimental result. In figure 10, we show a comparison of the experimental profile with the results of the simulation for values of p, 0.5 and 1, at time $t = 24$ h. We computed the χ^2 of the fit of density distributions for various values of p to the experimental one. It turns out that the smallest χ^2 is the one corresponding to $p = 1$. As a matter of fact, the ratio of χ^2 for $p = 0.5$ to $p = 1$ cases is 65. Moreover, we computed the χ^2 of the density fit of a cell distribution obtained with the second rule introduced in section 3, i.e. the cells move whenever possible even if this means violating the preference set by the probability threshold. The optimal value for this rule occurs close to $p = 0.5$. Still, the comparison of the χ^2 favours the first rule: the ratio of this χ^2 to that of the $p = 1$ previously obtained is 2.

We turn now to the inertia effect. In figure 11, we present this effect on the extreme case of $p = 1$ attraction. It is clear that the inclusion of this effect results in stronger diffusion of the cells. Comparing the density profiles to the experimental ones, we can conclude that a $p = 1$ attraction combined with the inertia effect does not improve the comparison with the experimental data. Indeed the ratio of χ^2 of the two fits is 41.

We complement our analysis by a study of the velocity distributions obtained in the simulation. A word of caution is necessary at this point. The time scale of 20 min used in the experimental study is particularly short: it corresponds to slightly over two updates of the automaton. Moreover, the use of a hexagonal lattice for the automaton imposes a motion of the centre of the cell of, minimally, a full cell diameter i.e. 35 μm in our model. Thus the comparison of the absolute values of the model velocities to the experimental ones is not particularly interesting. On the other hand, the ratio of the short- to long-interval mean velocities does have a meaning since it is a measure of the crookedness of the trajectory of the centre of mass of the cell. The value we have obtained

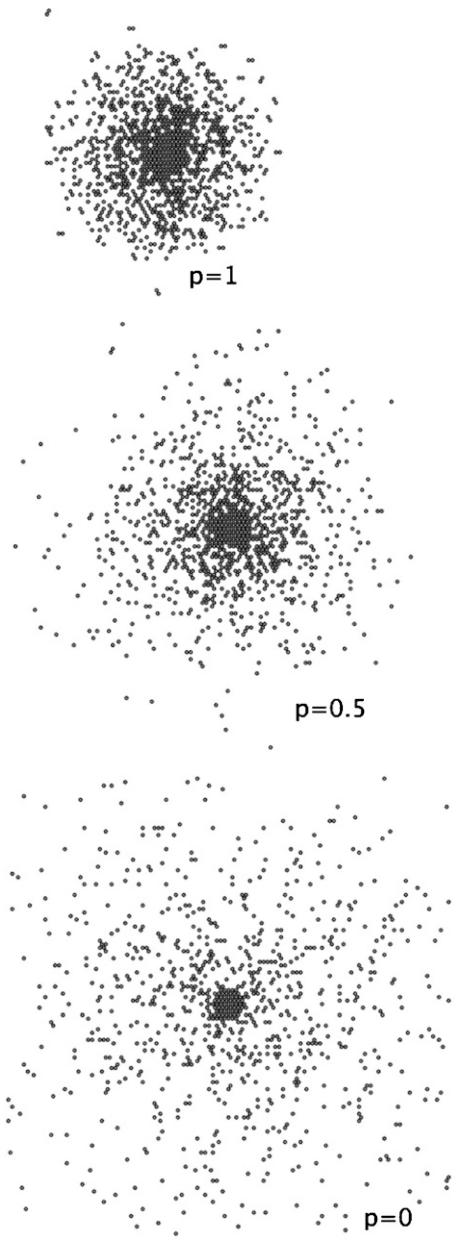

Figure 8. Cell migration patterns over 48 h, obtained from the automaton, for values of the probability threshold 1, 0.5 and 0, respectively.

for this quantity is 5.8 which is very close to that given by the experiment. At this point we must mention the result for the same ratio obtained with the variant of the attraction rule mentioned above: a value close to 2.3 was found, indicating much straighter trajectories.

As another interesting datum on the velocities, we have followed the cells ejected during the first 12 h and computed their mean velocities at the end of the 48 h evolution and present the velocities distribution in figure 12. At these times scales the distance covered by the cells is much longer than the minimal step in our model and thus the fact that the latter is equal to a full cell diameter will have a minimal effect on the velocities distribution. It would be interesting to compare data

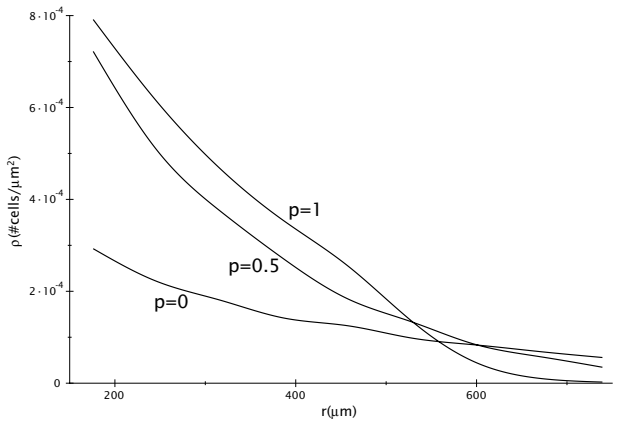

Figure 9. Density profiles over 36 h obtained for various values of the probability threshold.

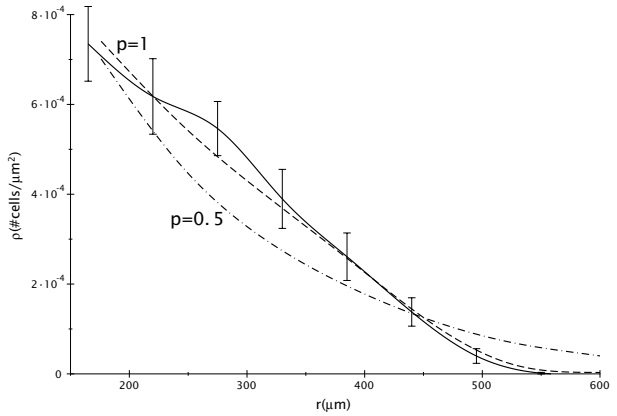

Figure 10. Comparison of the experimental data (after 24 h) with the results of the automaton for $p = 0.5$ and $p = 1$.

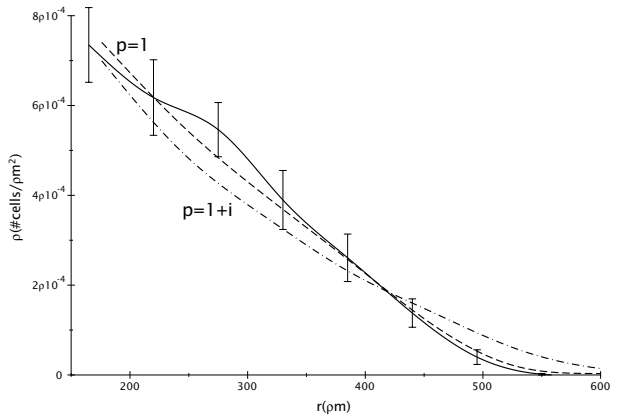

Figure 11. Comparison of the experimental data (after 24 h) with the results of the automaton for $p = 1$ with and without the inertia effect.

on velocities for this long-time evolution to experimental data (although the acquisition of the latter would be particularly difficult).

6. Conclusion and outlook

In this paper, we have presented a study of the migration properties of glioma cells in two dimensions over a collagen substrate. Our theoretical approach was based on a cellular automaton which models the migration of glioma cells and compared the theoretical results to experimental data previously obtained. Two rules were introduced in the automaton evolution, in order to simulate dynamical effects. The first is meant to reproduce cell attraction: the cells preferably move next to other cells (depending on a threshold as explained in section 3). From the fit of the experimental data it turns out that the best results are obtained for maximal attraction: the cells can *only* move next to other cells (otherwise they do not move). As explained above, this condition could account for different mechanisms such as cadherin or gap junction mediated attraction, or chemotaxis. A variant of this rule, where if there is no possible motion next to a neighbour the cell moves in a random direction, was also explored but it led to less satisfactory results. The other effect we investigated was that of inertia: the cells tend to move in a forward direction. The effect of inertia was rather small on the density profiles and it did not improve the overall fit.

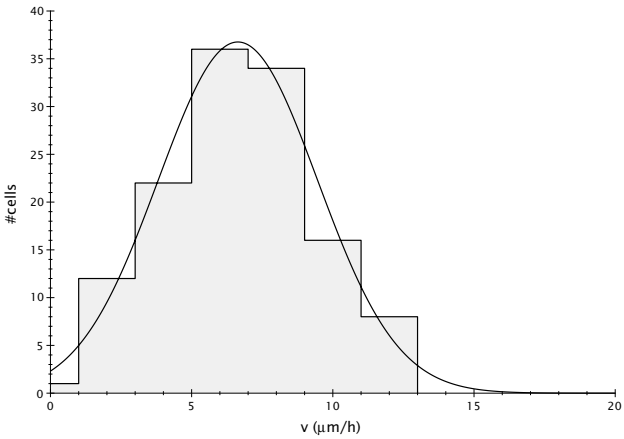

Figure 12. Histogram of the mean velocities of the cells ejected during the first 12 h, obtained after a 48 h evolution.

To conclude with our model of glioma cells migration, we find that there is an attraction between tumour cells based on chemotaxis or GJC. This attraction is necessary in order to reproduce the experimental data. This effect has as a consequence that our model differs from the diffusion migration i.e. the cells do not migrate randomly. Although this experiment is far from the *in vivo* situation, we believe that cell attraction could play a role in tumour growth.

We have also examined the velocity distributions of the cells. While the constraints of the migration on a lattice are non-negligible for short-time evolutions, it is interesting to note that the ratio of the long-to-short time-interval mean velocities is in fact in agreement with the experimental values. The latter is a good indicator of the convoluted character of the trajectory. Finally we have presented a histogram of the velocity distribution of the early-ejected cells at the end of 48 h. No experimental results exist yet for this quantity. It would be interesting to study these velocities and their evolution over time (both experimentally and theoretically) since we expect the migration, in the long run, to depend heavily upon them.

The system presented here is intentionally very simple. It has the advantage of limiting the number of biologically relevant parameters which are used in the model: only tumour cell–tumour cell interactions are involved. On the other hand, this system is far from the *in vivo* situation. In order to get closer to a realistic situation, we plan to extend our model so as to describe the migration of glioma cells in co-cultures with astrocytes. This more realistic situation will allow us to study the interaction between tumour cells in the presence of tumour cell–normal astrocytes interaction.

Glossary

Apoptosis. Programmed cell death. Cells commit suicide as a result of a signal.

Autocrine stimulus. Signal in response to secretion of a substance, like growth factor, that stimulates the secretory cell itself.

Box and ball. Cellular automaton system in which the evolution rules allow a single occupation of a given site, just like a game with balls and boxes in which one cannot put more than a single ball in each box.

Chemotaxis. Directed migration of cells controlled by a chemical gradient.

GL15. Human glioma cell line.

Glioma. Central nervous system tumour originated from glial cells.

Growth factor. Signalling molecule between cells that binds to specific receptors on the surface of a target cell and that activates cell differentiation, proliferation and even cell apoptosis.

Paracrine stimulus. Local signal in which a cell secretes a substance, like growth factor, that stimulates the cells in its neighbourhood without stimulating itself.

References

[1] Ferreira S C Jr, Martins M L and Vilela M J 2002 Reaction–diffusion model for the growth of avascular tumour *Phys. Rev.* E **65** 021907

[2] Kansal A R, Torquato S, Harsh G R IV, Chiocca E A and Deisboeck T S 2000 Simulated brain tumour growth dynamics using a three-dimensional cellular automaton *J. Theor. Biol.* **203** 367

[3] Burgess P K, Kulesa P M, Murray J D and Alvord E C Jr 1997 The interaction of growth rates and diffusion coefficients in a three-dimensional mathematical model of gliomas *J. Neuropathol. Exp. Neurol.* **56** 704

[4] Giuliano K A 1996 Dissecting the individuality of cancer cells: the morphological and molecular dynamics of single human glioma cells *Cell Motil. Cytosqueleton* **35** 237

[5] Sander L M and Deisboeck T S 2002 Growth patterns of microscopic brain tumours *Phys. Rev.* E **66** 051901

[6] Patel A A, Gawlinski E T, Lemieux S K and Gatenby R A 2001 A cellular automaton model of early tumour growth and invasion *J. Theor. Biol.* **213** 315

[7] Gatenby R A and Gawlinski E T 2003 The glycolytic phenotype in carcinogenesis and tumour invasion: insights through mathematical models *Cancer Res.* **63** 3847

[8] Giese A, Bjerkvig R, Berens M E and Westphal M 2003 Cost of migration: invasion of malignant gliomas and implications for treatment *J. Clin. Oncol.* **21** 1624

[9] Palfi S, Swanson K R, De Bouard S, Chretien F, Oliveira R, Gherardi R K, Kros J M, Peschanski M and Christov C 2004 Correlation of *in vitro* infiltration with glioma histological type in organotypic brain slices *Br. J. Cancer* **16** 745

[10] Swanson K R, Bridge C, Murray J D and Alvord E C Jr 2003 Virtual and real brain tumours: using mathematical modeling to quantify glioma growth and invasion *J. Neurol. Sci.* **216** 1

[11] Chicoine M R and Silbergeld D L 1995 Assessment of brain tumour cell motility *in vivo* and *in vitro J. Neurosurg.* **82** 615

[12] Hegedus B, Czirok A, Fazekas I, B'abel T, Madar'asz E and Vicsek T 2000 Locomotion and proliferation of glioblastoma cells *in vitro*: statistical evaluation of videomicroscopic observations *J. Neurosurg.* **92** 428

[13] Drasdo D and Hoehme S 2005 A single-cell-based model of tumour growth *in vitro*: monolayers and spheroids *Phys. Biol.* **2** 133

[14] Dormann S and Deutsch A 2002 Modeling of self-organized avascular tumour growth with a hybrid cellular automaton *Silico Biol.* **2** 35

[15] Zhang W, Couldwell W T, Simard M F, Song H, Lin J H and Nedergaard M 1999 Direct gap junction communication between malignant glioma cells and astrocytes *Cancer Res.* **59** 1994

[16] Oliveira R, Christov C, Guillamo J S, Bouard S De, Palfi S, Venance L, Tardy M and Peschanski M 2005 Contribution of gap junctional communication between tumour cells and astroglia to the invasion of the brain parenchyma by human glioblastomas *BMC Cell Biol.* **6** 7

[17] Guillamo J S, Lisovoski F, Christov C, Le Guerinel C, Defer G L, Peschanski M and Lefrancois T 2001 Migration pathways of human glioblastoma cells xenografted into the immunosuppressed rat brain *J. Neurooncol.* **52** 205

[18] De Bouard S, Christov C, Guillamo J S, Kassar-Duchossoy L, Palfi S, Leguerinel C, Masset M, Cohen-Hagenauer O, Peschanski M and Lefrancois T 2002 Invasion of human glioma biopsy specimens in cultures of rodent brain slices: a quantitative analysis *J. Neurosurg.* **97** 169

[19] Tokihiro T, Takahashi D, Matsukidaira J and Satsuma J 1996 From soliton equations to integrable cellular automata through a limiting procedure *Phys. Rev. Lett.* **76** 3247

[20] Perego C, Vanoni C, Massari S, Raimondi A, Pola S, Cattaneo M G, Francolini M, Vicentini L M and Pietrini G 2002 Invasive behaviour of glioblastoma cell lines is associated with altered organisation of the cadherin–catenin adhesion system *J. Cell Sci.* **115** 3331

[21] Huang R P, Hossain M Z, Sehgal A and Boynton A L 1999 Reduced connexin43 expression in high-grade human brain glioma cells *J. Surg. Oncol.* **70** 21

[22] Huang R P, Fan Y, Hossain M Z, Peng A, Zeng Z L and Boynton A L 1998 Reversion of the neoplastic phenotype of human glioblastoma cells by connexin 43 (cx43) *Cancer Res.* **58** 5089

[23] Lin J H *et al* 2002 Connexin 43 enhances the adhesivity and mediates the invasion of malignant glioma cells *J. Neurosci.* **22** 4302

[24] Deisboeck T S, Demuth T and Mansury Y 2005 Correlating velocity patterns with spatial dynamics in glioma cell migration *Acta Biotheor.* **53** 181

[25] Hegedus B, Czirok A, Fazekas I, B'abel T, Madar'asz E and Vicsek T 2000 Locomotion and proliferation of glioblastoma cells *in vitro*: statistical evaluation of videomicroscopic observations *J. Neurosurg.* **92** 428

[26] Chicoine M R and Silbergeld D L 1995 The *in vitro* motility of human gliomas increases with increasing grade of malignancy *Cancer* **75** 2904